analytical chemistry

pubs.acs.org/ac Article

Size Separation of Exosomes and Microvesicles Using Flow Field-Flow Fractionation/Multiangle Light Scattering and Lipidomic Comparison

Young Beom Kim, Gwang Bin Lee, and Myeong Hee Moon*

Cite This: *Anal. Chem.* 2022, 94, 8958−8965 Read Online

ACCESS | Metrics & More | Article Recommendations | Supporting Information

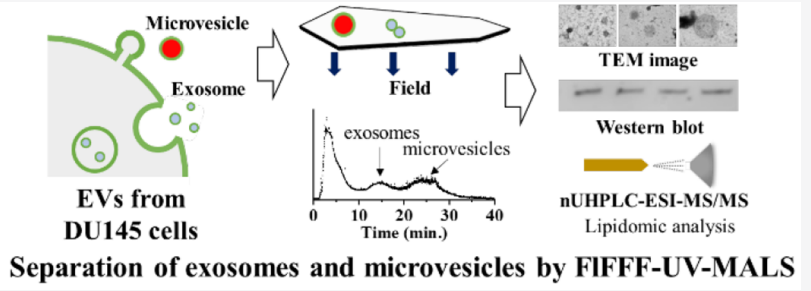

ABSTRACT: Extracellular vesicles (EVs) are cell-derived membrane-bound particles, including exosomes and microvesicles that differ in cellular origin, content, and lipid composition. This study reports that exosomes and microvesicles can be simultaneously separated by size using flow field-flow fractionation (FlFFF) employed with field programming and that the detection of low-concentration EV species can be significantly improved using multiangle light scattering (MALS). The efficiency of ultracentrifugation (UC) and ultrafiltration (UF) in isolating EVs from the culture media of DU145 cells was compared, and the results showed that UF retrieves more EVs than UC. Two size fractions (small and large) of both exosomes and microvesicles were collected during the FlFFF runs and examined using Western blotting to confirm each EV, and transmission electron microscopy was performed for size analysis. Sizes were compared using the root-mean-square radius obtained from the MALS calculation. The collected fractions were further examined using nanoflow ultrahigh-performance liquid chromatography-electrospray ionization-tandem mass spectrometry for the size-dependent lipidomic profiles of exosomes and microvesicles, showing that lipids were more enriched in the fraction containing large exosomes than in that containing small exosomes; however, an opposite trend was observed with microvesicles. The present study demonstrated that UF followed by FlFFF-MALS can be utilized for the size separation of exosomes and microvesicles without sequential centrifugation, which is useful for monitoring the changes in the size distribution of EVs depending on the biological status along with generating size-dependent lipidomic profiles.

Extracellular vesicles (EVs) are cell-derived nanometer-sized particles found in most body fluids and contain proteins, lipids, DNA, RNA, and signaling molecules.[1−3] EVs are composed of exosomes (30−100 nm in diameter), which are released by the fusion of multivesicular bodies with the plasma membrane, and microvesicles (100−1000 nm), which are formed by the outward budding of the plasma membrane.[4] Recently, EVs have attracted attention not only because of their roles in intercellular communications but also because of them being possible biomarkers for diseases and as potential carriers for RNA drugs.[5,6]

Because EVs are surrounded by a lipid bilayer to protect biomolecules in the inner aqueous core, the lipid composition and function of EVs are of interest in understanding EV biogenesis under various pathological conditions; however, this information is largely unknown. Lipids are essential components of biological membranes and are closely related to energy storage, cell signaling, and cell growth.[7,8] Lately, lipidomic analysis has been conducted on EVs derived from various cancer cell lines, human plasma, and urine.[9−11] Various types of membrane vesicles have been highlighted as biomarker candidates,[12,13] such as exosomes and microvesicles, which are similar in structure but differ in size, cellular origin, and lipid composition.[14,15] Therefore, it is challenging to separate or isolate exosomes and microvesicles and systematically examine their lipidomic profiles. Currently, methods commonly utilized to isolate EVs include ultracentrifugation (UC), ultrafiltration (UF), and size exclusion chromatography.[16,17] However, these

Received: February 18, 2022
Accepted: June 1, 2022
Published: June 13, 2022

https://doi.org/10.1021/acs.analchem.2c00806
Anal. Chem. 2022, 94, 8958−8965

techniques have some limitations: they are time-consuming and less efficient, and there is an overlap of unwanted subpopulations during the isolation of EVs from biofluids, including plasma and urine.[18−20] In particular, several studies revealed that high-speed centrifugation may induce aggregation or morphological changes of EVs, which may mislead EV characterization.[21,22] Moreover, separation of exosomes using UC cannot be completely achieved owing to the presence of microvesicles. Therefore, it is challenging to develop an appropriate method to separate exosomes and microvesicles under intact conditions.

Flow field-flow fractionation (FlFFF) is an elution-based separation method that is capable of fractionating nanometer- to micrometer-sized particles or proteins by differences in hydrodynamic diameters.[23−25] Separation in FlFFF is carried out in an unobstructed channel by employing two different flow streams: a migration flow moving along the channel axis to drive sample components toward the detector and a crossflow moving across the channel axis to retard the migration of sample components. Sample components in the FlFFF channel are forced by crossflow toward the channel wall, resulting in the particles distributing against the wall depending on their diffusion coefficients. Smaller particles with faster diffusion tend to be distributed further away from the channel wall than larger particles. When the migration flow of a parabolic flow pattern is applied, small particles elute earlier than larger ones, thus achieving size separation. As FlFFF utilizes an open channel space without packing materials and runs in a biological buffer solution for separation, it is suitable for handling biomolecules without the fear of the sample adhering to packing materials, as in chromatography. FlFFF has been widely utilized for the size separation of biological macromolecules such as proteins, lipoproteins, virus-like particles, subcellular species, and cells.[26−30] Efforts to separate EVs using FlFFF have been made with exosomes from several biological origins: urine from patients with prostate cancer,[31] cells,[32,33] and human plasma or serum.[34,35] The latter[35] showed that FlFFF coupled with multiangle light scattering (MALS) can resolve exosomes from lipoproteins in serum extracts prepared with UC and UF methods. A recent study demonstrated that hollow fiber FlFFF (HF5) and MALS can be powerfully utilized for the separation of EV subfractions prepared from differential UC methods and size characterization of large EVs (>100 nm).[36]

In this study, we utilized online FlFFF-MALS to demonstrate the simultaneous separation of cellular exosomes and microvesicles isolated using the UF method. Due to the possible aggregation or morphological changes of EVs using UC methods, UF can be an alternative to retrieve entire EV species simply. Fractions of exosomes and microvesicles were isolated from the culture media of DU145 cells using a series of centrifugation methods including UC as a reference and subjected to FlFFF-MALS for size separation in comparison. To minimize the possible aggregation or sample adhesion of EVs at the channel membrane during the focusing and relaxation procedure, a frit-inlet asymmetrical flow field-flow fractionation channel that utilizes hydrodynamic relaxation was employed for the separation of EVs with field programming for effective separation of EVs with a broad size. The particle sizes of exosomes and microvesicles were determined using MALS and compared with measured diameter values of the collected fractions obtained using transmission electron microscopy (TEM). Western blot analysis of the fractions collected during FlFFF runs was performed to identify exosomes and microvesicles. Lastly, size-dependent lipid profiles were examined for the two size fractions (small and large) of exosomes and microvesicles using nanoflow ultrahigh-performance liquid chromatography-electrospray ionization-tandem mass spectrometry (nUHPLC-ESI-MS/MS).

EXPERIMENTAL SECTION

Materials and Reagents. Sodium chloride (NaCl), sodium phosphate dibasic heptahydrate ($Na_2HPO_4{\cdot}7H_2O$), potassium chloride (KCl), potassium phosphate monobasic (KH_2PO_4), sodium dodecyl sulfate (SDS), sodium azide (NaN_3), ammonium formate (NH_4HCO_2), ammonium hydroxide (NH_4OH), chloroform ($CHCl_3$), and primary antibodies (rabbit-anti-CD40 and mouse-anti-α-tubulin) were purchased from Sigma-Aldrich (St. Louis, MO, USA). Primary (mouse-anti-ALIX, rabbit-anti-CD9, and rabbit-anti-HSP70), secondary (goat-anti-rabbit IgG H&L [HRP]), and rabbit anti-mouse IgG H&L [HRP]) antibodies were purchased from Abcam (Cambridge, UK). EZ-Western Lumi Femto solution was purchased from DoGenBio Co., Ltd. (Seoul, Korea). HPLC-grade water, acetonitrile (ACN), isopropyl alcohol (IPA), methanol (CH_3OH), and methyl *tert*-butyl ether (MTBE) were purchased from Avantor Performance Materials (Center Valley, PA, USA). Polystyrene standards with nominal diameters (22, 46, 102, 203, and 994 nm) were purchased from Thermo Fisher Scientific (Waltham, MA, USA). Fetal bovine serum (FBS) and penicillin/streptomycin for cell culture were purchased from System Bioscience LLC (Palo Alto, CA, USA). Thirty lipid standards used for the optimization of nUHPLC-ESI-MS/MS experiments and 19 lipid standards with odd-numbered and deuterated acyl chains as internal standards for targeted quantification were purchased from Avanti Polar Lipid Inc. (Alabaster, AL, USA) and listed in the Supporting Information (SI).

Cell Culture and EV Isolation. The DU145 HRPC cell line was obtained from the Korean Cell Line Bank (Seoul, Republic of Korea). The cells were cultured in RPMI 1640 medium (Invitrogen, Carlsbad, CA) supplemented with 10% exosome-depleted heat-inactivated FBS and 1% penicillin/streptomycin in 100 mm culture dishes at 37 °C in an incubator with a humidified atmosphere and 5% CO_2 for 72 h. The culture media of the harvested DU145 cells (approximately 2×10^5 cells/mL) were collected, and the EVs were isolated from the culture media using sequential centrifugation methods and UF as follows. The culture media from the three dishes (approximately 30 mL in total) were pooled. Pooled culture medium was centrifuged at 1,000 × *g* for 10 min to remove the cell debris, and the supernatant was centrifuged at 12,000 × *g* for 30 min at 4 °C to obtain microvesicle pellets. The final supernatant was transferred to a polycarbonate ultracentrifuge tube (Beckman Coulter Inc., Brea, CA, USA) and centrifuged at 120,000 × *g* for 2 h at 4 °C using an Optima XE-100 ultracentrifuge equipped with a Type 70 Ti rotor. The supernatant was removed to obtain an exosome pellet. Each pellet was resuspended in 0.01 M phosphate buffer saline (PBS) solution (100 μL for pellets E and M and 200 μL for pellet EV). Each suspension was vortexed for 10 min and stored at 4 °C. For the UF of EVs, the pooled culture media were centrifuged at 1,000 × *g* to remove cell debris, and the supernatant was filtered using a Vivaspin centrifugal concentrator (MWCO 300 kDa) from Sartorius AG (Goettingen, Germany). The retentate was transferred to a vial, vortexed,

https://doi.org/10.1021/acs.analchem.2c00806
Anal. Chem. 2022, 94, 8958−8965

and stored at 4 °C. The isolated EV suspensions were analyzed using FlFFF-UV-MALS.

FlFFF-UV-MALS. The FlFFF channel used for EV separation was a frit-inlet asymmetrical FlFFF channel modified in the laboratory. A 275 mm-long Eclipse channel from Wyatt Technology Europe GmbH (Dernbach, Germany) was utilized to assemble a frit-inlet asymmetrical FlFFF channel by replacing the depletion wall block with a polycarbonate inlay inserted with a small ceramic frit (35 mm × 18 mm × 7 mm) at the channel inlet end. The channel spacer was a 190 μm-thick Mylar sheet (26.6 cm in length and 2.2 cm wide at the inlet with a trapezoidal decrease to 0.6 cm wide at the outlet), and a regenerated cellulose membrane (MWCO 10 kDa) purchased from Wyatt Technology was utilized. The carrier solution used for polystyrene separation was prepared using deionized water (>18 MΩ·cm) with 0.05% SDS and 0.02% NaN_3 as bactericides. For EV separation, a 0.01 M PBS solution was prepared without adding sodium azide. All carrier solutions were filtered through a 0.1 μm-pore Durapore hydrophilic polyvinylidene fluoride (PVDF) membrane filter (Merck Millipore, Darmstadt, Germany) and degassed for 1 h for FlFFF analysis. Sample injection was performed using a model 7725i loop injector (200 μL loop) purchased from Rheodyne (Cotati, CA, USA) with an SP930D HPLC pump purchased from Young-Lin Instruments (Seoul, Korea). The frit flow was delivered to the frit inlet port using a model 1260 Infinity HPLC pump (Agilent Technologies, Palo Alto, CA, USA). The frit flow, outflow, and crossflow rates were controlled using an Eclipse Separation System (Wyatt Technology). During the field programming, the crossflow rate was linearly decayed, while the sample injection flow and outflow rates were fixed at 0.1 mL/min and 0.6 mL/min, respectively. During the field programming, the crossflow rate was initially maintained at 1.5 mL/min for 3 min, decreased linearly to 0.5 mL/min over 15 min, to 0.1 mL/min over 6 min, and to 0.02 mL/min over 3 min, and maintained at 0.02 mL/min until the end of the run. The eluted sample components were detected at a wavelength of 254 nm for PS standards and 280 nm for EVs using a model UV730D UV/vis detector (Young-Lin Instruments) and a model DAWN HELEOS II MALS detector (Wyatt Technology) at a wavelength of 658 nm. Detector signals were recorded using the ASTRA software (Wyatt Technology), and the root-mean-square (RMS) radius of EVs at each retention time frame was calculated using the Zimm approximation. During FlFFF of EV samples, two exosome fractions (10−14 and 14−18 min) and two microvesicle fractions (20−25 and 25−30 min) were collected for TEM, Western blotting, and lipid analysis using nUHPLC-ESI-MS/MS.

TEM and Western Blot Analysis of the Collected Fractions. Details of TEM and the Western blot analysis of exosomes and microvesicles of the FlFFF fractions are in the SI.

Lipid Extraction from EV Fractions. Extraction of lipids from the collected EV fractions was performed using MTBE/CH_3OH as previously described.[37] Each FlFFF fraction was concentrated to approximately 200 μL using an Amicon Ultra-15 Centrifugal Filter (30 kDa NMWL) and lyophilized. Each dried powder was then mixed with 300 μL of CH_3OH and placed in an ice bath. MTBE (1000 μL) was added to the mixture and vortexed for 1 h; to this mixture was added 250 μL of MS-grade water. The final mixture was vortexed for 10 min and centrifuged at 2,000 × g for 5 min. The upper organic layer was collected in a new 2 mL tube, and the remaining aqueous layer was mixed with 300 μL of MTBE/CH_3OH (10:3, v/v). The solution was vortexed for 10 min and centrifuged. The upper layer was mixed with the previously collected solution, and the final organic solution was dried in N_2 gas using an Evatros mini evaporator from Goojung Engineering (Seoul, Korea). Finally, the dried lipids were weighed and dissolved in $CHCl_3$:CH_3OH:H_2O (1:18:1, v/v) to a concentration of 5 μg/μL. A mixture of internal standards (ISs) was added to the lipid extract solution, and the lipid solution was stored at −80 °C until analysis.

nUHPLC-ESI-MS/MS Analysis of Lipids. Lipidomic analysis of EV fractions was performed using an nUHPLC-ESI-MS/MS composed of a Dionex Ultimate 3000 RSLCnano LC system coupled with a Q Exactive mass spectrometer from Thermo Fisher Scientific. For nUHPLC separation, an analytical column (7 cm × 100 μm, i.d.) was prepared in the laboratory by packing 1.7 μm BEH (ethylene-bridged hybrid) C18 particles (130 Å) into a pulled-tip capillary tube. BEH particles were unpacked from a BEH column (Waters, Milford, MA, USA), and the detailed procedure for column packing can be found in an earlier work.[38] Mobile phase solutions for lipid analysis were 9/1 (v/v) H_2O/ACN for mobile phase A and 7/1.5/1/0.5 IPA/CH_3OH/ACN/H_2O for B. Both were mixed with 5 mM HCO_2NH_4 and 5 mM NH_4OH as ionization modifiers that can be used for both positive and negative ion modes.[39] The gradient elution was initiated with 1% B, then increased to 70% B for 2 min, 80% B for 3 min, 90% B for 5 min, and 99% B for 10 min, and then maintained at 99% B for 10 min. Thereafter, the mobile phase composition was returned to 1% B for 5 min for column reconditioning, resulting in a total analysis duration of 35 min. The flow rate of the analytical column was adjusted to 800 nL/min, and the injection volume was 1 μL for all experiments. The ESI voltage was 3 kV for both ion modes, and the m/z range was set to 350−1100. To identify lipid molecules, the lipid extracts of each exosome and microvesicle group were pooled. Structural identification of the lipids was performed using the LipidMatch[40] software and manually confirmed by considering the retention time and MS/MS spectra. For targeted quantitative analysis of the lipids, the full MS scan mode was used in the polarity switching mode for alternate scanning in positive and negative ion modes. The quantification of each lipid was calculated as the relative peak area compared with that of the IS specific to each lipid species. The types of precursor ions, quantifier ions, and collision energy values assigned for different lipid classes for selected reaction monitoring (SRM) quantification are listed in Table S1. Statistical analysis was conducted by Student's t test using the SPSS software (version 26.0, IBM Corp., Armonk, NY, USA).

RESULTS AND DISCUSSION

FlFFF-UV-MALS of Extracellular Vesicles. The capability of FlFFF for the separation of EVs ranging from 30 to a few hundred nanometers was evaluated using polystyrene (PS) latex standards by applying field programming in which the crossflow rate ($\dot{V}_c$) decays during the run. Figure 1 shows the comparison of PS separations obtained at a) a constant field strength and b) a linear field decay program. Both runs were carried out at a fixed sample flow rate (or an injection flow rate, $\dot{V}_s$ = 0.1 mL/min) and an outflow rate (or a detector flow rate, $\dot{V}_{out}$ = 0.6 mL/min). Because the present study utilized a frit inlet asymmetrical FlFFF channel, the frit flow rate ($\dot{V}_f$)

https://doi.org/10.1021/acs.analchem.2c00806
Anal. Chem. 2022, 94, 8958−8965

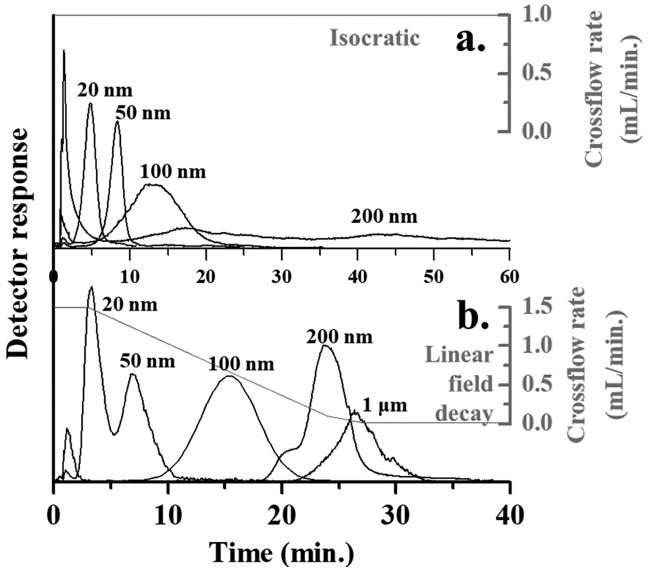

Figure 1. Fractograms of polystyrene standards by flow field-flow fractionation (FlFFF) at a) a constant field strength (crossflow rate ($\dot{V}_c$ = 1.0 mL/min) and b) a linear field decay program ($\dot{V}_c$ = 1.5 decreased to 0.02 mL/min) obtained at a sample flow rate/outflow rate ($\dot{V}_s/\dot{V}_{out}$) = 0.1/0.6 mL/min. The frit flow rate ($\dot{V}_f$) was adjusted as $\dot{V}_c + \dot{V}_{out} - \dot{V}_s$.

was adjusted as $\dot{V}_f = \dot{V}_c + \dot{V}_{out} - \dot{V}_s$. When the field strength was fixed, PS particles smaller than 100 nm were well resolved, as shown in Figure 1a; however, 200 nm PS particles appeared to be very broad and barely separated. Employment of a programmed field decay pattern was successful in resolving particles of one order of diameter (20−200 nm) with some loss in resolution for particles larger than 200 nm. The application of a higher initial field strength (initial $\dot{V}_c$ = 1.5 mL/min) followed by field decay was necessary to provide sufficient force to resolve the lower size limit of exosomes (~30 nm) from numerous proteins or small molecules that may contaminate the exosome fraction and facilitate the elution of large-diameter particles (~ a few hundred nanometers) presumed to be microvesicles.

EV fractions of the DU145 cell culture media were prepared by sequential centrifugation and UF, as illustrated in Scheme 1 based on the isolation methods for exosomes and microvesicles that were reported in the literature,[16,18,19,36] and run by FlFFF-UV-MALS under the same conditions used in Figure 1b, in which the FlFFF channel was online coupled to the UV detector and MALS in sequence. Figures 2a and 2b show the fractograms of pellets E and M illustrated with the UV and MALS (90°) signals for comparison. All collected pellets were resuspended in the PBS solution for FlFFF analysis, and the injection volume used was 100 μL for the three pellet samples. Figure S1 of SI shows the reproducibility of FlFFF separation for these EV fractions with the superimposed fractograms of five repeated injections of each pellet sample. According to the isolation procedures described in the literature, pellets E and M are expected to contain exosomes and microvesicles, respectively. The intense peak signals observed before 5 min in the fractograms of Figures 2a and 2b are expected to be smaller species, including vesicles smaller than 20 nm or proteins that coprecipitated during centrifugation. While UV signals of pellets E and M in Figures 2a and 2b, respectively, were very weak or negligible in distinguishing the elution of

Scheme 1. Isolation Schemes of Extracellular Vesicles Based on Centrifugation Methods[a] and Ultrafiltration with a 300 kDa Membrane (UF 300) from Culture Media of DU145 Cells

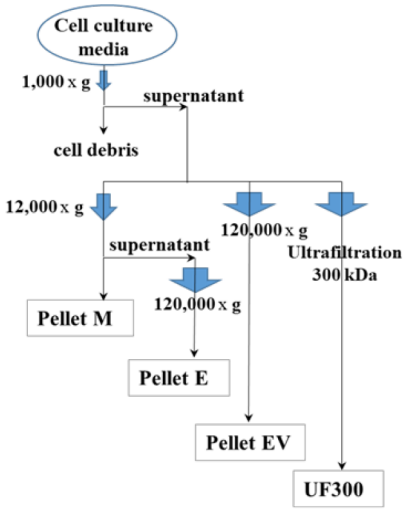

[a]Pellet M stands for microvesicles, pellet E stands for exosomes, and pellet EV stands for whole extracellular vesicles.

vesicles with the present injection amount, the MALS signals of both fractions were able to clearly confirm the elution of EVs at different retention time regimes. The number of cells corresponding to 100 μL of suspension for each pellet (E and M) was approximately 6 × 10^6. Above the MALS detector signals of pellets E and M, the root-mean-square (RMS) radius values calculated from MALS and UV signals showed a steady increase with increased retention time for both pellet samples, demonstrating the successful size separation of FlFFF. The average RMS radius values were 34.6 nm for the Exo-S fraction, 60.6 nm for the Exo-L fraction, 121.1 nm for the MV-S fraction, and 338.2 nm for the MV-L fraction (Table 1), supporting the normal mode of FlFFF separation.

The TEM images of the collected fractions (Figure 2c) distinctly showed the size differences between the two collected fractions, and the average diameter values measured from the TEM images are listed in Table 1. RMS radius values were based on MALS signals at time intervals corresponding to each fraction. While TEM images reflect the geometric size of dried EVs, the RMS radius from the MALS calculation refers to the mass distribution-based size of EVs dispersed in solution. Therefore, the sizes measured from the TEM images are not directly comparable with the RMS radius values. However, size results from both methods in Table 1 show the same trend of increases upon retention time with some deviations. In a previous study,[35] a good agreement was shown between the results from TEM and dynamic light scattering (DLS) calculations of exosome fractions although DLS measurements were based on the diffusion coefficients of particles. EV fractions collected during the FlFFF runs were analyzed by Western blotting using antibodies specific for exosomes (Alix, HSP70, and CD9)[14,41,42] and microvesicles (CD40 and α-tubulin)[43,44] (Figure 2d). Alix, a protein associated with endosomal sorting complexes required for transport, participates in the formation of intraluminal vesicles, which are released into the exosome,[45] and HSP70 is a heat-shock protein known as a well-known exosome marker.[46]

https://doi.org/10.1021/acs.analchem.2c00806
Anal. Chem. 2022, 94, 8958−8965

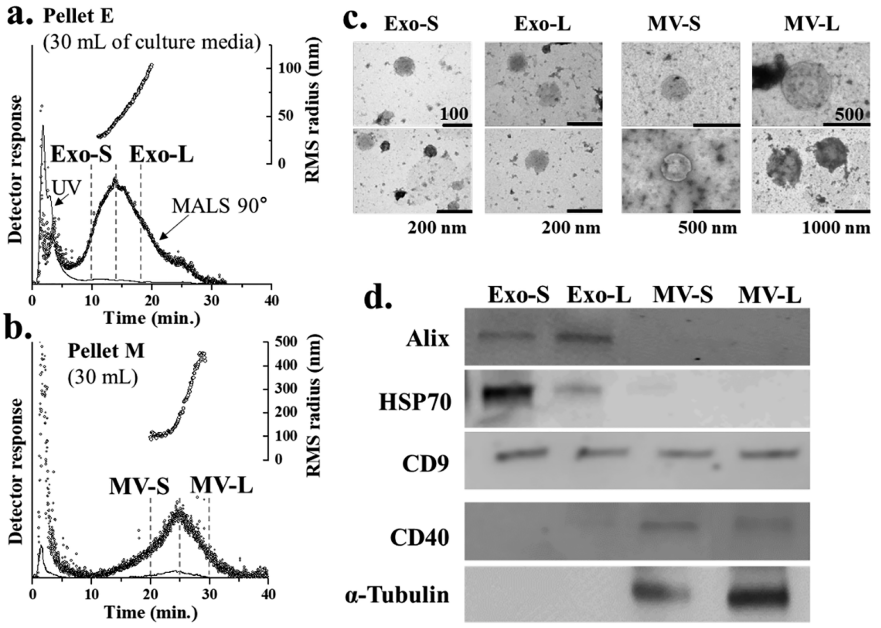

Figure 2. FlFFF fractograms (superimposed with UV and MALS-90° signals) of a) pellet E (exosome fraction) and b) pellet M (microvesicle fraction) along with the plots of RMS radius values from MALS. c) TEM images of the small and large size fractions (Exo-S and Exo-L for exosomes and MV-S and MV-L for microvesicles) and d) Western blot results with the exosome markers (ALIX, HSP70, and CD9) and microvesicle markers (CD40 and α-tubulin).

Table 1. Comparison between the Average Radius Measured from TEM Images and the RMS Radius Calculated from MALS Based on the Zimm Method for the Collected Size Fractions of Exosomes and Microvesicles

fraction	time (min)	RMS radius (nm)	TEM radius (nm)	count
Exo-S	10.0−14.0	34.6 ± 5.0	26.5 ± 5.2	29
Exo-L	14.0−18.0	60.6 ± 10.0	57.8 ± 7.8	16
MV-S	20.0−25.0	121.1 ± 23.2	146.7 ± 27.8	11
MV-L	25.0−30.0	338.2 ± 85.7	397.0 ± 73.0	8

While Alix and HSP70 were detected in the Exo-S and Exo-L fractions, confirming the presence of exosomes, they were not detected in either of the microvesicle fractions. This agrees with the observations on exosomes from DU145 cell lines in the literature.[47] Although CD9 and CD40 are membrane proteins, CD9 is known to be enriched in both exosomes and microvesicles, but CD40 has been reported as a marker for microvesicles.[48,49] Moreover, CD9 was present in all fractions along with the exclusive finding of CD40 in the two microvesicle fractions. α-Tubulin, a microvesicle marker, was detected only in two microvesicle fractions. The present results agree with the finding that a CD9 antibody responded to both exosomes and microvesicles from plasma, while α-tubulin was specific to microvesicles.[50] From the Western blot results, it was confirmed that exosomes and microvesicles were successfully separated by FlFFF without significant contamination by the other.

Figure 3 demonstrates the capability of FlFFF to resolve exosomes and microvesicles prepared using the UC and UF methods. Figure 3a shows the elution of pellet EV, which is the entire sediment by UC at 120,000 × g after removing the cell debris and represents a similar elution pattern as observed in Figures 2a and 2b; however, their separation was not achieved at the baseline level. Figure 3a was obtained with a reduced amount of culture media extract injection, which was half of

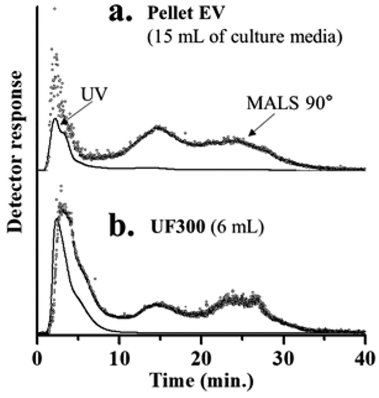

Figure 3. FlFFF fractograms (UV and MALS-90° signals) of a) pellet EV and b) the UF300 sample obtained using FlFFF-UV-MALS. Volume information in the parentheses of each sample represents the volume equivalent to the original culture media.

the volume injected for pellets E and M. The intensity scale of all FlFFF fractograms in Figure 3 was the same as used in Figure 2. To bypass the use of UC to isolate EVs from cell culture media, a UF method was employed for the supernatant after initially removing the cell debris using a simple centrifuge at 1,000 × g. For the UF300 fraction, 30 mL of pooled media was concentrated 30-fold (1 mL) using a UF membrane filter (300 kDa), and 200 μL of the UF300 extracts (equivalent to 6 mL of the culture media) was injected into the FlFFF. The intense peak observed at 2−8 min (Figure 3b) was expected to originate from small-sized EVs or proteins that were not completely removed using UF. These small components were expected to be larger than 300 kDa. However, the intensity of the main peaks eluted after 10 min was similar to that of pellet EV, indicating that the isolation efficiency of EVs from UF with a 300 kDa membrane was higher than that of UC (15 mL vs 6

https://doi.org/10.1021/acs.analchem.2c00806
Anal. Chem. 2022, 94, 8958−8965

mL of the culture media). This result was similar to the earlier results observed with exosomes.[35] More interestingly, the peak intensity of the microvesicles of the UF extracts was higher than that of exosomes at 10−20 min (Figure 3b), which was the opposite of the observation with pellet EV (Figure 3a). This supports the fact that UF not only provides a higher efficiency for the isolation of EVs than UC but also minimizes the loss of microvesicles. The reason to use different volumes of the culture media was the difficulty in concentrating the retentate of the EV solution by UF due to the viscous nature, and the injection of 100 μL of the UF retentate was equivalent to about 6 mL of the culture media. While UF preparation of EVs retains large amounts of smaller species, FlFFF can differentiate these species from EV targets by its size separation capability. Although UV signals (which were concentration dependent) of the resuspended EV pellet and the UF300 fraction were very weak, light scattering signals (dependent on the concentration and molar mass of sample species) were intense, confirming the separation of exosomes and microvesicles by size. It is clear now that UF followed by FlFFF analysis can be useful for the isolation and analysis of exosomes and microvesicles simultaneously without UC, which may induce aggregation during the isolation of EVs.

Lipidomic Analysis of EV Fractions. Lipid profiles in the two size fractions of exosomes and microvesicles were analyzed using nUHPLC-ESI-MS/MS. The performance of lipid separation in both positive and negative ion modes of nUHPLC-ESI-MS/MS is demonstrated by the base peak chromatograms (BPCs) of lipid standards in Figure S2 of the SI. The lipid extract samples (1 μL each) from each size fraction were injected for lipid analysis, and the BPCs of the lipid extracts from the four collected fractions are shown in Figure S3. From nontargeted lipid identification of the four EV fractions, a total of 1,257 lipid species were identified based on their molecular structures from the collision-induced dissociation (CID) spectra. Among them, 1,106 species were identified from the exosome fractions (Exo-S and Exo-L), 1,132 species were identified from the microvesicle fractions (MV-S and MV-L), and 981 species were commonly detected in both groups. The majority of the identified lipid classes was triacylglycerols (TGs) (795 for exosomes and 764 for microvesicles), followed by phosphatidylcholines (PCs) (58 for exosomes and 106 for microvesicles). Quantitative analysis of lipids from each fraction was performed using the identified lipid targets by injecting the same amount of extracted lipids for each fraction. Quantified results of 292 lipid species are expressed as normalized lipid amounts (relative to an internal standard (IS) specific to each lipid class) along with the relative abundance of each lipid class in Table S2. Because lipid quantification was based on the total number of carbon and double bonds in acyl chains, lipids with different isomeric structures were not differentiated. The isomeric structures of PC, PE, PA, PG, PI, PS, DG, TG, and CL species of exosomes and microvesicles were identified using CID spectra and are listed in Table S3.

The distribution of lipid classes was compared between the small- and large-sized EVs using the pie chart in Figure 4, showing that the total lipid level of the large size fraction of exosomes (Exo-L) increased by approximately 50% compared to that of Exo-S, while the total lipid level of large microvesicles (MV-L) decreased by 22% compared to that of MV-S. This finding supports the hypothesis that more lipids accumulate in larger exosomes and smaller microvesicles. An earlier study[32]

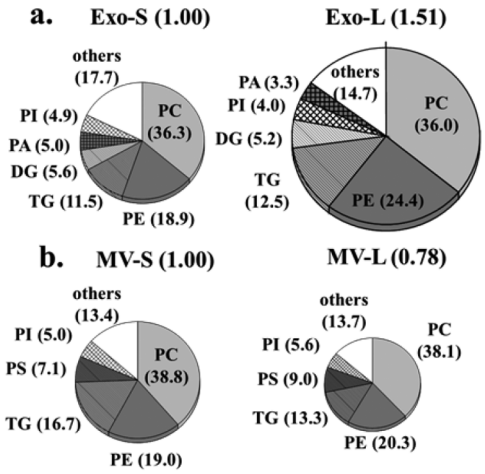

Figure 4. Pie charts showing the relative composition of lipid classes in the small and large size groups of a) pellet E (exosomes) and b) pellet M (microvesicles) based on the total concentration of each lipid class. Only the high abundance lipid classes were plotted, and the remaining classes were represented as a summed amount marked with "others". The numbers in the parentheses of L are relative to that of *S* set to 1.00.

characterizing exosomes by size using FlFFF had reported that the amount of lipids in large-diameter exosomes was higher than that in smaller ones. At the lipid class level, the relative occupancies of PC, TG, and DG were not significantly different between the fractions of exosomes, whereas PE was enriched in Exo-L (24.4%) more than Exo-S (18.9%), but PA and PI were depleted by more than 20%. In the case of microvesicles, the total levels of PC, PE, and PI were not significantly different by sizes, but those of TG and PS were depleted and enriched by ∼20%, respectively, in the MV-L group. Detailed plots of the changes in lipid class levels between the two size groups are shown in Figure S4.

Lipid profiles at the molecular level were compared using stacked bar graphs in Figure 5, in which the highly abundant species were annotated with information on their acyl chain structure. The levels of LPC (largely from LPC 18:0) and LPA (LPA 18:0) were largely depleted in the large size fractions of both exosomes and microvesicles. In the case of PA and PS, their levels were not dependent on vesicle size; however, the most highly abundant PA species (PA 34:1, 36:1, 36:2, and 38:4) were enriched in exosomes by more than 2-fold compared to that in microvesicles, but most PS species (PS 34:1, 36:1, 36:2, and etc.) were enriched in microvesicles than in exosomes by more than 3-fold. Studies have shown that microvesicles are enriched with PS, and exposing the outer membrane on the cell surface to PS is related to the release of microvesicles.[51,52] PC, PE, DG, and TG classes were enriched in the large size fraction of exosomes (Exo-L), while they showed an opposite trend in microvesicles. The remaining lipid classes did not show significant differences in lipid content with size (Figure S5). As the size-dependent lipid profiles of exosomes and microvesicles have rarely been studied, the relationship between lipid distribution and the size of exosomes and microvesicles remains unclear. Nonetheless, the present study shows that there is a clear difference in the level of certain lipid classes depending on the vesicle size for both exosomes and microvesicles, but their trends are different from each other, implying differences in their cellular origin and roles.

https://doi.org/10.1021/acs.analchem.2c00806
Anal. Chem. 2022, 94, 8958−8965

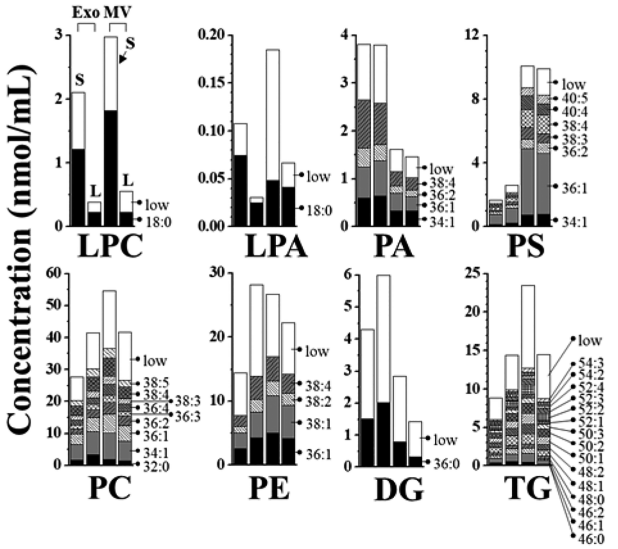

Figure 5. Stacked bar graphs showing compositional differences of each lipid class represented with the level of individual lipid species (in nmol/mL) in the small (S) and large (L) size fractions of pellets E and M. The numbers (e.g., 18:0) at each bar represent the acyl chain structure of highly abundant species in each lipid class. The "low" category represents the summed amounts of species with low abundance.

CONCLUSIONS

This study demonstrated that cellular exosomes and microvesicles can be sorted by size using FlFFF with programmed decay of the crossflow rate and that the size-dependent lipid profiles of EV fractions can be investigated using nUHPLC-ESI-MS/MS. The detection of EV species present at low concentrations was enhanced using MALS, and the size differences between exosomes and microvesicles were confirmed with RMS radius distributions. Although few studies have been conducted on the differences in lipid accumulation and pathways according to EV size, further studies on size-dependent lipid distribution in EVs derived from other cell types are required to confirm this observation. Regardless, the simultaneous separation of exosomes and microvesicles may offer the possibility to monitor changes in vesicle size and the relative distribution of these EVs using FlFFF without UC. The present study also demonstrated that both UC and UF methods can be utilized for the initial isolation of EVs from cell culture media prior to FlFFF separation of exosomes and microvesicles; however, UF was found to be more efficient than UC. Moreover, the developed method can be utilized for the selective detection of lipid targets or specific biomarkers contained in exosomes or microvesicles by employing direct hyphenation of FlFFF with ESI-MS/MS. As real-time differentiation of specific lipids in EVs using FlFFF-ESI-MS/MS may reveal the biological status of cells and biofluids, including blood, urine, and even saliva, it will be promising for high-speed screening or diagnosis of pathological lipid components.

ASSOCIATED CONTENT

Supporting Information

The Supporting Information is available free of charge at https://pubs.acs.org/doi/10.1021/acs.analchem.2c00806.

List of lipid standards; TEM and Western blot analysis of collected fractions; fractograms of repeated injections from pellets E and M by FlFFF; BPCs of lipid standards in positive and negative ion modes of nUHPLC-ESI-MS/MS; BPCs of small (S) and large (L) size fractions of pellets E and M obtained at positive and negative ion modes of nUHPLC-ESI-MS/MS; total amounts of each lipid class in two different size fractions of exosomes and microvesicles; stacked bar graphs of each lipid class not shown in Figure 5; list of lipid standards utilized for targeted quantification; normalized lipid amount (vs IS) of lipid species from small and large size fractions of exosomes and microvesicles; and isomeric structures of phospholipids identified from exosomes (E) and microvesicles (M) (PDF)

AUTHOR INFORMATION

Corresponding Author

Myeong Hee Moon − *Department of Chemistry, Yonsei University, Seoul 03722, South Korea;* orcid.org/0000-0002-5454-2601; Phone: (82) 2 2123 5634; Email: mhmoon@yonsei.ac.kr; Fax: (82) 2 364 7050

Authors

Young Beom Kim − *Department of Chemistry, Yonsei University, Seoul 03722, South Korea*

Gwang Bin Lee − *Department of Chemistry, Yonsei University, Seoul 03722, South Korea*

Complete contact information is available at: https://pubs.acs.org/10.1021/acs.analchem.2c00806

Notes

The authors declare no competing financial interest.

ACKNOWLEDGMENTS

This study was supported by a grant from the National Research Foundation (NRF) of Korea (NRF-2021R1A2C2003171).

REFERENCES

(1) Van Niel, G.; d'Angelo, G.; Raposo, G. *Nat. Rev. Mol. Cell Biol.* **2018**, *19* (4), 213−228.

(2) Kalra, H.; Drummen, G. P.; Mathivanan, S. *Int. J. Mol. Sci.* **2016**, *17* (2), 170.

(3) Tetta, C.; Ghigo, E.; Silengo, L.; Deregibus, M. C.; Camussi, G. *Endocrine.* **2013**, *44* (1), 11−19.

(4) Raposo, G.; Stoorvogel, W. *J. Cell Biol.* **2013**, *200* (4), 373−383.

(5) De Jong, O. G.; Van Balkom, B. W.; Schiffelers, R. M.; Bouten, C. V.; Verhaar, M. C. *Front. immunol.* **2014**, *5*, 608.

(6) Alvarez-Erviti, L.; Seow, Y.; Yin, H.; Betts, C.; Lakhal, S.; Wood, M. J. *Nat. Biotechnol.* **2011**, *29* (4), 341−345.

(7) Wenk, M. R. *Cell.* **2010**, *143* (6), 888−895.

(8) Shevchenko, A.; Simons, K. *Nat. Rev. Mol. Cell Biol.* **2010**, *11* (8), 593−598.

(9) Brzozowski, J. S.; Jankowski, H.; Bond, D. R.; McCague, S. B.; Munro, B. R.; Predebon, M. J.; Scarlett, C. J.; Skelding, K. A.; Weidenhofer, J. *Lipids Health Dis.* **2018**, *17* (1), 211.

(10) Sun, Y.; Saito, K.; Saito, Y. *Metabolites.* **2019**, *9* (11), 259.

(11) Kreimer, S.; Belov, A. M.; Ghiran, I.; Murthy, S. K.; Frank, D. A.; Ivanov, A. R. *J. Proteome Res.* **2015**, *14* (6), 2367−2384.

(12) Sun, Y.; Huo, C.; Qiao, Z.; Shang, Z.; Uzzaman, A.; Liu, S.; Jiang, X.; Fan, L.-Y.; Ji, L.; Guan, X. *J. Proteome Res.* **2018**, *17* (3), 1101−1107.

(13) Ohno, S.-i.; Ishikawa, A.; Kuroda, M. *Adv. Drug Delivery Rev.* **2013**, *65* (3), 398−401.

(14) Haraszti, R. A.; Didiot, M.-C.; Sapp, E.; Leszyk, J.; Shaffer, S. A.; Rockwell, H. E.; Gao, F.; Narain, N. R.; DiFiglia, M.; Kiebish, M. A. *J. Extracell. Vesicles.* **2016**, *5* (1), 32570.
(15) Durcin, M.; Fleury, A.; Taillebois, E.; Hilairet, G.; Krupova, Z.; Henry, C.; Truchet, S.; Trötzmüller, M.; Köfeler, H.; Mabilleau, G. *J. Extracell. Vesicles.* **2017**, *6* (1), 1305677.
(16) Momen-Heravi, F.; Balaj, L.; Alian, S.; Mantel, P.-Y.; Halleck, A. E.; Trachtenberg, A. J.; Soria, C. E.; Oquin, S.; Bonebreak, C. M.; Saracoglu, E. *Biol. Chem.* **2013**, *394* (10), 1253−1262.
(17) Furi, I.; Momen-Heravi, F.; Szabo, G. *Ann. Transl. Med.* **2017**, *5* (12), 263.
(18) Witwer, K. W.; Buzás, E. I.; Bemis, L. T.; Bora, A.; Lässer, C.; Lötvall, J.; Nolte-'t Hoen, E. N.; Piper, M. G.; Sivaraman, S.; Skog, J. *J. Extracell. Vesicles.* **2013**, *2* (1), 20360.
(19) Li, P.; Kaslan, M.; Lee, S. H.; Yao, J.; Gao, Z. *Theranostics.* **2017**, *7* (3), 789.
(20) Yuana, Y.; Levels, J.; Grootemaat, A.; Sturk, A.; Nieuwland, R. *J. Extracell. Vesicles.* **2014**, *3* (1), 23262.
(21) Erdbrugger, U.; Rudy, C. K.; Etter, M. E.; Dryden, K. A.; Yeager, M.; Klibanov, A. L.; Lannigan, J. *Cytometry A* **2014**, *85* (9), 756−70.
(22) Linares, R.; Tan, S.; Gounou, C.; Arraud, N.; Brisson, A. R. *J. Extracell. Vesicles.* **2015**, *4* (1), 29509.
(23) Giddings, J. C. *Science.* **1993**, *260* (5113), 1456−1465.
(24) Wahlund, K. G.; Giddings, J. C. *Anal. Chem.* **1987**, *59* (9), 1332−1339.
(25) Moon, M. H. *TrAC, Trends Anal. Chem.* **2019**, *118*, 19−28.
(26) Yang, J. S.; Lee, J. Y.; Moon, M. H. *Anal. Chem.* **2015**, *87* (12), 6342−6348.
(27) Rambaldi, D. C.; Reschiglian, P.; Zattoni, A.; Johann, C. *Anal. Chim. Acta* **2009**, *654* (1), 64−70.
(28) Chen, Y.; Zhang, Y.; Zhou, Y.; Luo, J.; Su, Z. *Vaccine.* **2016**, *34* (27), 3164−3170.
(29) Kang, D.; Oh, S.; Reschiglian, P.; Moon, M. H. *Analyst.* **2008**, *133* (4), 505−515.
(30) Giddings, J. C.; Yang, F. J.; Myers, M. N. *Anal. Biochem.* **1977**, *81* (2), 395−407.
(31) Yang, J. S.; Lee, J. C.; Byeon, S. K.; Rha, K. H.; Moon, M. H. *Anal. Chem.* **2017**, *89* (4), 2488−2496.
(32) Zhang, H.; Freitas, D.; Kim, H. S.; Fabijanic, K.; Li, Z.; Chen, H.; Mark, M. T.; Molina, H.; Martin, A. B.; Bojmar, L. *Nat. Cell Biol.* **2018**, *20* (3), 332−343.
(33) Yang, J. S.; Kim, J. Y.; Lee, J. C.; Moon, M. H. *Anal. Chim. Acta* **2019**, *1073*, 79−89.
(34) Wu, B.; Chen, X.; Wang, J.; Qing, X.; Wang, Z.; Ding, X.; Xie, Z.; Niu, L.; Guo, X.; Cai, T. *Anal. Chim. Acta* **2020**, *1127*, 234−245.
(35) Kim, Y. B.; Yang, J. S.; Lee, G. B.; Moon, M. H. *Anal. Chim. Acta* **2020**, *1124*, 137−145.
(36) Marassi, V.; Maggio, S.; Battistelli, M.; Stocchi, V.; Zattoni, A.; Reschiglian, P.; Guescini, M.; Roda, B. *J. Chromatogr. A* **2021**, *1638*, 461861.
(37) Byeon, S. K.; Lee, J. Y.; Moon, M. H. *Analyst.* **2012**, *137* (2), 451−458.
(38) Lee, J. C.; Park, S. M.; Kim, I. Y.; Sung, H.; Seong, J. K.; Moon, M. H. *Biochim. Biophys. Acta - Mol. Cell Biol. Lipids.* **2018**, *1863* (9), 980−990.
(39) Bang, D. Y.; Lim, S.; Moon, M. H. *J. Chromatogr. A* **2012**, *1240*, 69−76.
(40) Koelmel, J. P.; Kroeger, N. M.; Ulmer, C. Z.; Bowden, J. A.; Patterson, R. E.; Cochran, J. A.; Beecher, C. W.; Garrett, T. J.; Yost, R. A. *BMC bioinform.* **2017**, *18* (1), 331.
(41) Kowal, J.; Tkach, M.; Théry, C. *Curr Opin Cell Biol.* **2014**, *29*, 116−125.
(42) Zhang, G.; Liu, Z.; Ding, H.; Zhou, Y.; Doan, H. A.; Sin, K. W. T.; Zhu, Z. J.; Flores, R.; Wen, Y.; Gong, X. *Nat. Commun.* **2017**, *8* (1), 589.
(43) Théry, C.; Ostrowski, M.; Segura, E. *Nat. Rev. Immunol.* **2009**, *9* (8), 581−593.
(44) Menck, K.; Scharf, C.; Bleckmann, A.; Dyck, L.; Rost, U.; Wenzel, D.; Dhople, V. M.; Siam, L.; Pukrop, T.; Binder, C. *J. Mol. Cell Biol.* **2015**, *7* (2), 143−153.
(45) Baietti, M. F.; Zhang, Z.; Mortier, E.; Melchior, A.; Degeest, G.; Geeraerts, A.; Ivarsson, Y.; Depoortere, F.; Coomans, C.; Vermeiren, E. *Nat. Cell Biol.* **2012**, *14* (7), 677−685.
(46) Clayton, A.; Turkes, A.; Navabi, H.; Mason, M. D.; Tabi, Z. *J. Cell Sci.* **2005**, *118* (16), 3631−3638.
(47) Hosseini-Beheshti, E.; Choi, W.; Weiswald, L.-B.; Kharmate, G.; Ghaffari, M.; Roshan-Moniri, M.; Hassona, M. D.; Chan, L.; Chin, M. Y.; Tai, I. T. *Oncotarget.* **2016**, *7* (12), 14639.
(48) Bobrie, A.; Colombo, M.; Krumeich, S.; Raposo, G.; Théry, C. *J. Extracel. Vesicles.* **2012**, *1* (1), 18397.
(49) Fraser, K.; Jo, A.; Giedt, J.; Vinegoni, C.; Yang, K. S.; Peruzzi, P.; Chiocca, E. A.; Breakefield, X. O.; Lee, H.; Weissleder, R. *Neuro-oncology.* **2019**, *21* (5), 606−615.
(50) Menck, K.; Bleckmann, A.; Schulz, M.; Ries, L.; Binder, C. *J. Vis. Exp.* **2017**, No. 119, No. e55057.
(51) Heijnen, H. F.; Schiel, A. E.; Fijnheer, R.; Geuze, H. J.; Sixma, J. J. *Blood* **1999**, *94* (11), 3791−3799.
(52) Muralidharan-Chari, V.; Clancy, J. W.; Sedgwick, A.; D'Souza-Schorey, C. *J. Cell Sci.* **2010**, *123* (10), 1603−1611.

https://doi.org/10.1021/acs.analchem.2c00806
Anal. Chem. 2022, 94, 8958−8965